Title

Endoluminal ultrasound applicators for MR-guided thermal ablation of pancreatic tumors: Preliminary design and evaluation in a porcine pancreas model

Journal

Medical Physics, 43(7)

ISSN

0094-2405

Authors

Adams, Matthew S
Salgaonkar, Vasant A
Plata-Camargo, Juan
et al.

Publication Date

2016-07-01

DOI

10.1118/1.4953632

Peer reviewed

Endoluminal ultrasound applicators for MR-guided thermal ablation of pancreatic tumors: Preliminary design and evaluation in a porcine pancreas model

Matthew S. Adams[a)]
Thermal Therapy Research Group, University of California, San Francisco, 2340 Sutter Street, S341, San Francisco, California 94115 and The UC Berkeley - UCSF Graduate Program in Bioengineering, University of California, Berkeley, and University of California, San Francisco, California 94115

Vasant A. Salgaonkar
Thermal Therapy Research Group, University of California, San Francisco, 2340 Sutter Street, S341, San Francisco, California 94115

Juan Plata-Camargo
Department of Radiology, Stanford University, Stanford, California 94305

Peter D. Jones
Thermal Therapy Research Group, University of California, San Francisco, 2340 Sutter Street, S341, San Francisco, California 94115

Aurea Pascal-Tenorio
Department of Comparative Medicine, Stanford University, Stanford, California 94305

Hsin-Yu Chen
The UC Berkeley - UCSF Graduate Program in Bioengineering, University of California, Berkeley, and University of California, San Francisco, California 94115

Donna M. Bouley
Department of Comparative Medicine, Stanford University, Stanford, California 94305

Graham Sommer and Kim Butts Pauly
Department of Radiology, Stanford University, Stanford, California 94305

Chris J. Diederich
Thermal Therapy Research Group, University of California, San Francisco, 2340 Sutter Street, S341, San Francisco, California 94115 and The UC Berkeley - UCSF Graduate Program in Bioengineering, University of California, Berkeley, and University of California, San Francisco, California 94115

(Received 6 January 2016; revised 3 May 2016; accepted for publication 26 May 2016; published 15 June 2016)

Purpose: Endoluminal ultrasound may serve as a minimally invasive option for delivering thermal ablation to pancreatic tumors adjacent to the stomach or duodenum. The objective of this study was to explore the basic feasibility of this treatment strategy through the design, characterization, and evaluation of proof-of-concept endoluminal ultrasound applicators capable of placement in the gastrointestinal (GI) lumen for volumetric pancreas ablation under MR guidance.
Methods: Two variants of the endoluminal applicator, each containing a distinct array of two independently powered transducers (10×10 mm 3.2 MHz planar; or $8\times10\times20$ mm radius of curvature 3.3 MHz curvilinear geometries) at the distal end of a meter long flexible catheter assembly, were designed and fabricated. Transducers and circulatory water flow for acoustic coupling and luminal cooling were contained by a low-profile polyester balloon covering the transducer assembly fixture. Each applicator incorporated miniature spiral MR coils and mechanical features (guiding tips and hinges) to facilitate tracking and insertion through the GI tract under MRI guidance. Acoustic characterization of each device was performed using radiation force balance and hydrophone measurements. Device delivery into the upper GI tract, adjacent to the pancreas, and heating characteristics for treatment of pancreatic tissue were evaluated in MR-guided *ex vivo* and *in vivo* porcine experiments. MR guidance was utilized for anatomical target identification, tracking/positioning of the applicator, and MR temperature imaging (MRTI) for PRF-based multislice thermometry, implemented in the real-time RTHawk software environment.
Results: Force balance and hydrophone measurements indicated efficiencies of 48.8% and 47.8% and −3 dB intensity beam-widths of 3.2 and 1.2 mm for the planar and curvilinear transducers, respectively. *Ex vivo* studies on whole-porcine carcasses revealed capabilities of producing ablative temperature rise ($\Delta T > 15$ °C) contours in pancreatic tissue 4–40 mm long and 4–28 mm wide for the planar transducer applicator (1–13 min sonication duration, ~4 W/cm^2 applied acoustic intensity). Curvilinear transducers produced more selective heating, with a narrower $\Delta T > 15$ °C contour length

and width of up to 1–24 mm and 2–7 mm, respectively (1–7 min sonication duration, ~4 W/cm^2 applied acoustic intensity). Active tracking of the miniature spiral coils was achieved using a Hadamard encoding tracking sequence, enabling real-time determination of each coil's coordinates and automated prescription of imaging planes for thermometry. *In vivo* MRTI-guided heating trials in three pigs demonstrated capability of ~20 °C temperature elevation in pancreatic tissue at 2 cm depths from the applicator, with 5–7 W/cm^2 applied intensity and 6–16 min sonication duration. Dimensions of thermal lesions in the pancreas ranged from 12 to 28 mm, 3 to 10 mm, and 5 to 10 mm in length, width, and depth, respectively, as verified through histological analysis of tissue sections. Multiple-baseline reconstruction and respiratory-gated acquisition were demonstrated to be effective strategies in suppressing motion artifacts for clear evolution of temperature profiles during MRTI in the *in vivo* studies.

Conclusions: This study demonstrates the technical feasibility of generating volumetric ablation in pancreatic tissue using endoluminal ultrasound applicators positioned in the stomach lumen. MR guidance facilitates target identification, device tracking/positioning, and treatment monitoring through real-time multislice PRF-based thermometry. © *2016 American Association of Physicists in Medicine.* [http://dx.doi.org/10.1118/1.4953632]

Key words: endoluminal ultrasound, thermal ablation, pancreatic cancer, MR-guided intervention, MRTI

1. INTRODUCTION

Thermal ablation is currently being investigated as a treatment option for patients suffering from advanced pancreatic ductal adenocarcinoma (PDAC). Thermal destruction of tumor tissue may slow down disease progression to extend survival[1,2] and can alleviate pain and other symptoms through tumor debulking and neurolysis/denervation mechanisms.[3,4] Many ablative techniques have been developed and clinically evaluated for treatment of PDAC, including RF ablation, microwave ablation, high-intensity focused ultrasound (HIFU), cryoablation, and laser ablation, among others.[1,5] Minimally invasive interstitial-based techniques have resulted in high complication rates due to inadvertent damage of surrounding sensitive structures to the tumor, including bowel tissues, normal pancreas, biliary structures, or major vasculature.[6,7] Lower morbidity and mortality have been established by using these techniques in a more invasive open-surgery setting, with additional precautions, such as endoluminal cooling of adjacent gastrointestinal (GI) lumens, to protect against undesirable thermal injury.[5] MRI or US guided extracorporeal HIFU offers a noninvasive means of ablating tumor tissue, but relies on clear acoustic transmission into the tumor site.[8,9] This is often obstructed by intervening organs or gas-filled bowel in close proximity to the pancreas, particularly around the pancreatic head region.[10,11]

Endoluminal and intracavitary catheter-based ultrasound applicators can potentially provide a minimally invasive and effective means of ablating tumors adjacent to the gastrointestinal tract. Catheter-based ultrasound possesses many advantages compared to other ablative technologies, including the high degree of control over the spatial deposition of acoustic energy through transducer design, direct localization of energy delivery to the target region, and compatibility with imaging modalities, such as ultrasound or MRI, for direct treatment feedback.[12] In consideration of treating PDAC, endoluminal ultrasound could serve as a less invasive and inherently safer alternative to traditional RFA and MWA interstitial techniques and may also circumvent accessibility issues associated with extracorporeal HIFU, in particular for target regions close to the GI tract. Specific configurations of endoluminal ultrasound applicators have been developed for delivering ablation to GI-accessible sites, including the biliary tract,[13] esophagus,[14] and liver.[15,16] For ablating pancreas and liver tissue from the stomach lumen, an endoscope with an integrated miniature spherically focused HIFU transducer [12 mm diameter, 35 mm radius of curvature (ROC), 3.73 MHz] has been developed and experimentally verified in *in vivo* porcine studies.[17] This device demonstrated feasibility of creating small (~3 × 10 mm) lesions beyond the stomach wall that were sequentially delivered with ~30 s sonication durations and illustrated the utility of integrated endoscopic ultrasound to guide positioning and monitor bubble formation as an indicator for ablation.[17]

Ultrasound[18] and MRI (Refs. 19 and 20) can be used to guide and monitor thermal therapy treatments in real-time and provide a means to enhance the accuracy of energy deposition and directly verify the efficacy of treatment delivery. Advantages of MR guidance include improved targeting due to enhanced soft-tissue contrast and generation of multiple tomographic temperature maps across arbitrary planes using MR temperature imaging (MRTI), thereby providing direct and volumetric feedback to treatment progress. MRTI has been paired with many ablative modalities and recently has been used in conjunction with extracorporeal HIFU for ablation of pancreatic body tumors in patients with locally advanced PDAC.[10]

The principal aim of this study is to assess the general feasibility of using an MR-compatible endoluminal ultrasound applicator to generate thermal ablation of pancreatic tissue from the GI lumen under MR guidance, as shown in Fig. 1. In contrast to spherically or highly focused HIFU, emphasis was placed on designing applicators capable of volumetric thermal coverage, as appropriate for the large

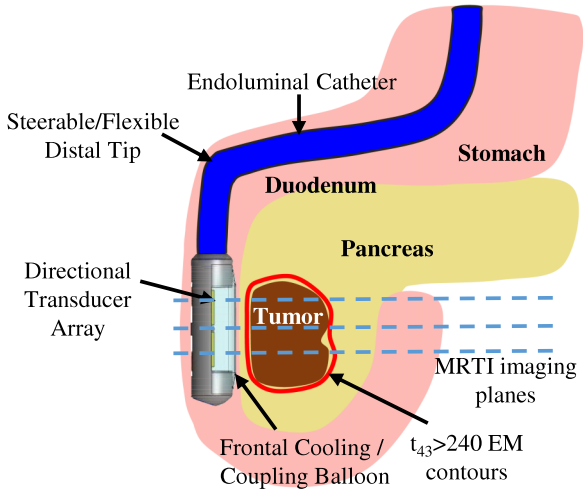

FIG. 1. Schema and concepts of an endoluminal ultrasound applicator positioned in the GI tract for thermal therapy of pancreatic tumors. The applicator is illustrated as positioned in the duodenum for sonication of tumors in the head of the pancreas, following placement and insertion strategies common in endoscopy. Transducer arrays are configured for lightly focused or diffuse patterns to provide a high degree of spatial control and volumetric heating.

size of advanced primary pancreatic tumors,[21] and in order to minimize repositioning requirements and take advantage of MRTI multislice capabilities. Here we report the technical design of the proof-of-concept (POC) applicators, results of acoustic characterizations and preliminary delivery, and performance assessments in exploratory MR-guided *ex vivo* and *in vivo* heating trials in porcine animal models.

2. METHODS

2.A. Endoluminal ultrasound applicator fabrication

Two configurations of endoluminal applicators, incorporating different transducer geometries, were designed and fabricated. One applicator incorporated a two-element array of planar 10 × 10 mm gold-plated piezoceramic transducers (EBL #1, EBL Products, Inc.), operating at a frequency of 3.2 MHz; the second contained a two-element array of lightly curvilinear 8 × 10 mm gold-plated piezoceramic transducers (EBL #1, EBL Products, Inc.), with an operating frequency of 3.3 MHz and 20 mm ROC along the short dimension. Transducer assembly fixtures for the distal tip of the applicator were designed for each configuration in SolidWorks, as shown in Fig. 2. The fixtures contain two rectangular channels for seating each transducer, ports for wiring, internal channels for circulatory water flow, and attachment ports to the body and tip of the applicator. The dimensions of the cylindrical fixture were 12 mm OD and 45 mm length, conservatively chosen to accommodate passage through gastrointestinal anatomy.

The transducer fixtures were 3D printed in Veroclear material using an Objet260 Connex (Stratasys, Ltd.). Transducers were secured using Stycast 2651 epoxy (Henkel Electronics Materials) over the corresponding channels of the fixture for air-backing. A fixed-shape low-profile (radius = 7 mm) balloon made from 0.025 mm thick polyethylene terephthalate (PET) (Advanced Polymers, Inc.) was secured to the top of the fixture to cover the transducers and contain circulatory water flow. Approximately 1 m of nylon tubing (8 mm OD × 6 mm ID, McMaster-Carr) was used for the body of the applicator. Polyethylene tubing (1.4 mm ID, Becton, Dickinson, and Company) and coaxial cabling (Molex, Inc.) served for circulatory water flow and power transmission to the transducers, respectively, and were routed within the nylon body. On the proximal end of the applicator, Redel RF power connectors (Lemo S.A.) and luer connectors (Quosina Corporation) for water flow were attached. Active MR tracking coils, based off a spiral surface coil design[22] with four turns, ID ~ 1–1.5 mm and OD ~ 4 mm, were fabricated using silver wire (0.1 mm OD, California Fine Wire Company) and secured to the two platforms on the underside of each transducer fixture. Coaxial cables (Molex, Inc.) terminating with BNC connectors were attached to the coils. To improve maneuverability through the GI tract, a preshaped 6–8 cm long polyurethane (6.4 mm OD, Cole-Parmer) tip was secured to the distal end of the applicator, and a flexible pivot point made from silicone tubing (9.5 mm OD, HelixMark) was incorporated 3 cm proximal of the transducer stage fixture. Photos of the POC endoluminal ultrasound applicators are shown in Fig. 3.

2.B. Acoustic characterization

The mounted transducers on the fully assembled endoluminal ultrasound applicators were characterized using (1)

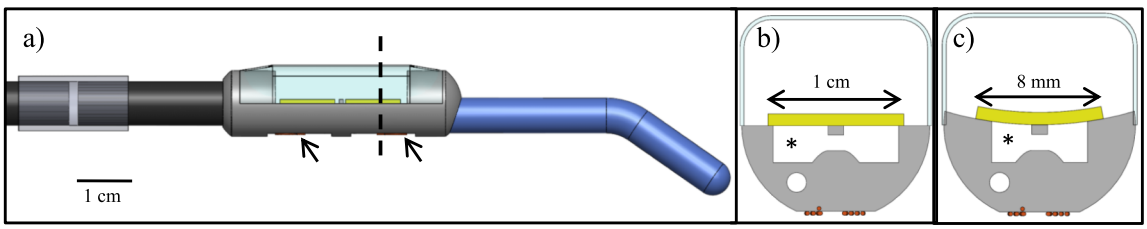

FIG. 2. (a) Design schematic of the distal tip of the endoluminal ultrasound applicator, featuring the transducer assembly fixture, which consists of a two-element transducer array (yellow) seated along the device length covered by a thin-walled PET balloon, and active MR tracking coils on the fixture underside (arrows). Maneuverability and tracking into the GI tract are enhanced by the distal polyurethane tip (blue) and proximal silicone hinge (gray). Cross sections along the dashed line through the assembly fixture are shown for the (b) planar and (c) curvilinear configurations, showing transducer dimensions and seating over the air-backed channels (asterisks). (See color online version.)

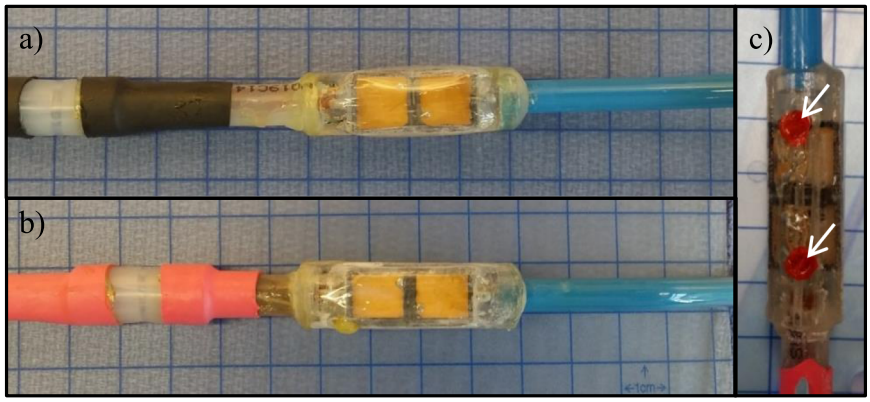

FIG. 3. Top-down views of constructed POC endoluminal ultrasound applicators containing (a) two 1 × 1 cm planar transducers at 3.2 MHz and (b) two 8 × 10 cm 20 mm ROC curvilinear transducers at 3.3 MHz. (c) Two spiral tracking coils (arrows) for active MR tracking were integrated on the backside of each transducer assembly fixture.

force balance measurements[23] to determine acoustic output power and efficiencies and (2) hydrophone measurements to map acoustic beam profiles across axial and sagittal planes relative to the mounted transducers. Force balance was performed using a bottom-loading mass balance (BP2100S, Sartorius AG) setup, with the applicator under test submerged in deionized and degassed water, directing acoustic energy into acoustic absorbers on the balance. The acoustic output power was calculated using the mass displacement, and the acoustic efficiency was calculated as the ratio of acoustic power to net electrical power (range: 5–25 W) delivered to both transducers, as measured using a power meter (438 A, Hewlett-Packard). Beam intensity distributions were characterized by placing the applicator under test in a tank filled with deionized, degassed water and scanning a needle-type hydrophone (Onda HNP-0400, Onda Corp.) under motor control along the $X-Z$ (axial) and $Y-Z$ (sagittal) planes. Step sizes were 0.25 mm for the X and Y axes and 0.5 mm along the Z (depth) axis. The pulse repetition rate for sonication was 1 ms, and burst count was 250 cycles. The peak-to-peak voltage measurements from the hydrophone were measured using an oscilloscope (AFG3022C, Tektronix, Inc.) and squared to obtain pressure-squared distributions, which were then normalized to the maximum value and represent normalized beam intensity distributions.

2.C. MRI experimental setup and RTHawk software platform

A 3T GE Discovery MRI scanner was used for all MR-guided experiments. Electronics for delivering RF power and cooling water flow were kept in the control room outside the MR suite. A function generator (HP Agilent 33220A) and RF amplifier (E&I Model 240L, Electronics & Innovation) were used to drive the transducers, with forward and reflected power monitored using an inline power meter (4391A, Bird Technologies). To reduce interference noise in the MRI images from the driving electronics, high power low pass filters (Model YA-1, Bencher, Inc.) and custom-built isolation transformers were integrated along the power lines to the shielded penetration panel of the MR suite. Shielded RF cabling was used to connect RF power lines to the applicator in the MR suite. Circulatory water flow was driven through the applicator PET balloon using a peristaltic pump (Masterflex, Cole-Palmer). Direct cooling of the water flow was achieved using an inline copper tubing heat-exchanger that was submerged in an ice-bath immediately proximal to the applicator input. Imaging was performed either with a phased-array cardiac coil (GE) or with two or three 13 or 20 cm surface coils connected to the scanner using a custom five-channel adapter and hardware. This second configuration enabled connections and active tracking capabilities of the two miniature RF coils integrated onto the underside of the applicator transducer fixture using a Hadamard encoding tracking sequence (TE = 2 ms, TR = 4 ms, FOV = 30 cm, and sample = 512),[24] which incorporated dithering along six orthogonal directions to reduce bulk noise.[25]

The RTHawk software environment (HeartVista, Inc.) was integrated with the GE scanner to provide real-time multislice continuous imaging and reconstruction capabilities, while allowing instant changes to pulse sequence parameters and imaging plane position and orientation. For thermometry purposes, a PRF-based GRE sequence (TE = 8 ms, TR = 23 ms, flip angle = 15, FOV = 30 cm, 128 × 128 acquisition matrix, and slice thickness = 5 mm) was implemented in RTHawk and provided multislice temperature monitoring at an update time of ~3 s/slice. Baseline images were acquired immediately after circulating flow was initiated (to incorporate any positional or flow-related artifact into the baseline) and prior to power delivery and used to subtract the baseline phase for temperature reconstruction during the course of heating. Background temporal phase drift was monitored in an ROI outside of the heated region and used to correct temperature calculations.[26] For improved target contrast, an IR-FSE sequence (TI = 729 ms, TE = 120 ms, TR = 1285.7 ms, flip angle = 90, echo train length = 24, FOV = 30 cm, 256 × 256 acquisition matrix, slice thickness = 7 mm, and NEX = 1) was also implemented in the RTHawk environment and used to confirm final positioning of the device and prescription of thermometry slices before the start of sonication.

2.D. Device characterization in MR-guided *ex vivo* porcine cadaver experiments

In order to validate applicator delivery strategies and characterize heating performance within the GI tract, six heating experiments were performed with six ~40 kg whole pig cadavers (euthanized from previous experiments within 12–24 h and kept in cold storage prior to study) within a 3 T GE MRI scanner. Given the onset of rigor mortis, and hence the lack of access through the mouth, the esophagus was surgically accessed prior to each experiment. The POC endoluminal applicator under test was introduced into the esophagus and directed into the stomach. High resolution T2-weighted FRFSE sequences (TE = 103 ms, TR = 3000–9000 ms, flip angle = 111, echo train length = 15, FOV = 30 cm, 512 × 512 acquisition matrix, slice thickness = 3 mm, and NEX = 2) were used to delineate the anatomy, the position of the device, and to identify the target region of the pancreas. Under guidance of the real-time imaging capabilities of the RTHawk platform, fine manual manipulation (translation, rotation) of the endoluminal applicator to the target position in the stomach adjacent to pancreatic tissue was performed. If targets within the pancreatic tissue could not be defined, the liver adjacent to the stomach was used as a surrogate target tissue instead. Temperature monitoring slices were prescribed using two approaches: manually, using a scout scan in the RTHawk interface to localize the applicator and determine alignment or automatically using the coordinates of the two active tracking coils.[27] One thermometry slice was positioned sagittal to the applicator transducer fixture to visualize the longitudinal extent of heating, and one to three were prescribed along the axial plane through the transducer stage. All slices were 5 mm in thickness with 1 mm gap between parallel slices, chosen to capture planes through the center of each transducer and the transducer assembly fixture. Sonications were performed for 5–13 min duration, at 3.8–5 W/cm^2 applied acoustic surface intensity. The heat-exchanger was placed in ice slurry to cool circulating water temperature during sonication, and circulatory water flow was set at a rate of 50–70 ml/min, resulting in a cooling water temperature of ~4.5 °C in the applicator. Due to the low baseline core temperature of the cadavers, which would preclude representative thermal lesion formation for the achieved temperature elevations, no excision or gross inspection of treated tissues following each study was performed.

2.E. MR-guided *in vivo* porcine experiments

Preliminary investigations of the applicator placement strategy, heating generation, and thermometry motion-compensation techniques were performed with *in vivo* heating

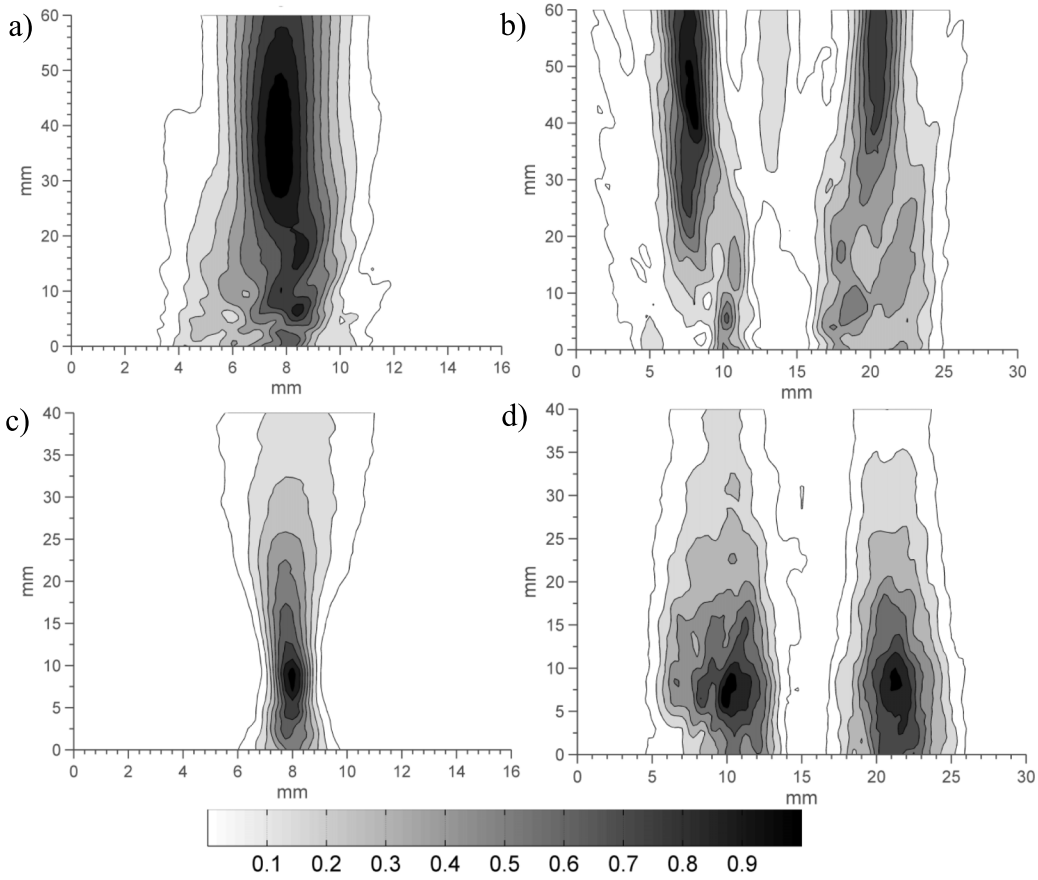

FIG. 4. Normalized pressure-squared distributions in degassed water for the [(a) and (b)] 3.2 MHz dual-planar and [(c) and (d)] 3.3 MHz dual-curvilinear applicators across the [(a) and (c)] axial and [(b) and (d)] sagittal planes, as measured using a hydrophone.

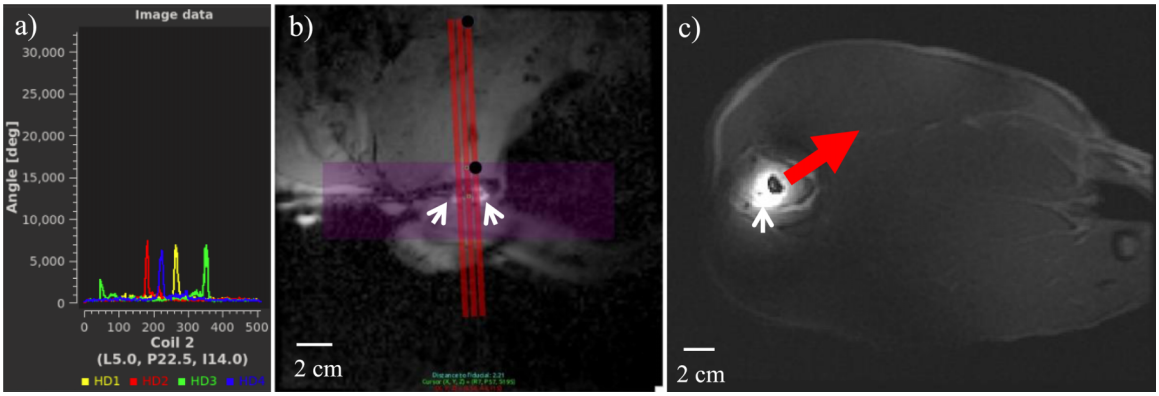

FIG. 5. (a) The 3D coordinates of the tracking coils were localized using a Hadamard encoded tracking sequence to obtain four projections of the coil signal. (b) Tracking coils (white arrows) could be visualized on the fixture and used to automatically prescribe imaging planes through the transducer stage. (c) Orientation of the applicator and direction of sonication (red arrow) could be determined by the relation between the hyperintense coil signal (white arrow) and hypointense applicator body.

trials within three adult female White York porcines (weight: 43–51 kg). All animal experiments and procedures were approved by Stanford IACUC. For each experiment, the animal was anesthetized with atropine (0.05 mg/kg) and Telazol (5 mg/kg), and maintained on isoflurane gas inhalation and controlled respiration for the duration of the experiment. Vital signs were continuously monitored. The animal was placed in the MRI scanner in dorsal or left lateral recumbency to facilitate device delivery into the stomach. The cardiac phased-array coil (chosen to obtain high SNR for image guidance and thermometry) was positioned around the proximal abdomen of the animal, closely centered to the region of the pancreas. The endoluminal applicator under test was inserted through the oral cavity into the esophagus to the stomach. Scout and T2-weighted anatomical scans were used for initial localization of the applicator and pancreas. Real-time imaging feedback (<1 s update time) with RTHawk was used for fine manual manipulation to positions within the stomach adjacent to the splenic lobe of the pancreas. Once the applicator was in position, imaging plane thermometry was prescribed and ice cooled water flow was set to a rate of 70 ml/min just prior to the start of sonication.

Two different strategies for performing thermometry in the presence of respiratory motion were implemented and evaluated. The first scheme integrated multislice MRTI (with one slice sagittal and up to three axial with respect to the device) acquired continuously during the course of heating with a multiple-baseline[29] reconstruction strategy. A library of ~20 reference baseline images was acquired prior to the onset of heating. Matching of temperature phase maps with the appropriate baseline was performed by determining the maximum intercorrelation coefficient between the target region of the corresponding anatomical image and the set of baseline images.[30] Breath-holds (30–60 s duration) were induced just prior to heating to obtain baselines (30 s with flow off and 30 s with flow on) and every subsequent 4 min following the start of heating in order to further minimize baseline misregistration and validate the reconstruction. The second thermometry scheme consisted of a single-slice with gated acquisition, using pressure bellows wrapped around the chest of the animal and connected to the MRI scanner. No breath-holds were induced, and while the GRE thermometry sequence was continuously prescribed so steady-state was achieved, data for a temperature image were only acquired and saved at the onset of expiration for each respiratory cycle. All MRTI images were thresholded to remove temperature measurements for the pixels with lowest (1%–10%) signal intensity magnitude, and rectangular spatial filters, centered on the applicator and target region, were used to isolate device-related heating.

After the sonications were complete, the applicator was withdrawn and the animal was removed from the MRI scanner and euthanized following protocol procedures. The pancreas and stomach were removed in necropsy and sectioned in order to measure and photograph dimensions of the gross lesions, defined by hyperemic border or tissue blanching. Transverse and longitudinal sections through the pancreatic lesions were harvested, fixed in formalin, routinely processed for paraffin embedding, and 4 μm-thick sections were adhered to glass slides and stained using hematoxylin and eosin (H&E) for histological analysis of the tissue structure.

3. RESULTS

3.A. Acoustic characterization

The acoustic efficiencies of the combined transducers were $48.8\% \pm 1.9\%$ for the planar applicator and $47.8\% \pm 0.5\%$ for the curvilinear applicator. The normalized acoustic beam pressure-squared distributions for each applicator are shown in Fig. 4 for longitudinal and transverse planes. Pressure-squared distributions were smoothed using a 3×3 pixel Gaussian filter, with a sigma value of 0.8. For the curvilinear applicator, the dimensions of the −3 dB beam-width are 1.2 mm along the focused dimension and extend 25 mm in depth, while for the planar applicator the −3 dB contour beam-width extends 3.2 mm.

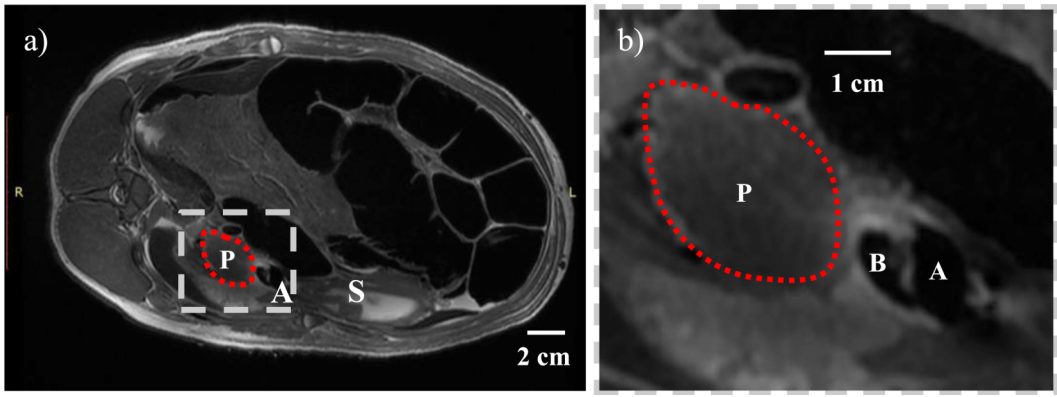

FIG. 6. (a) Placement of the dual-planar endoluminal ultrasound applicator **A** in *ex vivo* porcine stomach lumen **S** adjacent to pancreatic tissue **P** (bordered by the red dotted line). (b) ~3.5× magnified image showing axial cross section of the transducer assembly fixture **A** with frontal coupling balloon **B** aligned with and facing pancreatic tissue **P**.

3.B. Device characterization in MR-guided *ex vivo* porcine cadaver experiments

As shown in Fig. 5, the Hadamard encoded tracking sequence enabled determination of each coil's 3D coordinates in the scanner, permitting automatic prescription of imaging planes through the transducer stage for monitoring thermometry. The tracking coils could also be directly visualized with a GRE sequence and used to determine the orientation of the applicator. Alternatively, when using the phased-array cardiac coil, the device position and orientation could be determined from the characteristic hypointense profile of the transducer assembly fixture.

Applicator insertion into the stomach and placement against the stomach wall for treatment of adjacent pancreatic tissue, as demonstrated in Fig. 6, were achieved in five out of six total porcine cadaver experiments. Multislice temperature profiles for endoluminal sonications of pancreatic tissue using the planar and curvilinear applicators in separate experiments are shown in Figs. 7 and 8, respectively. Treatment parameters and MRTI measurements are shown for each carcass heating trial in Table I. For the planar applicator, potentially

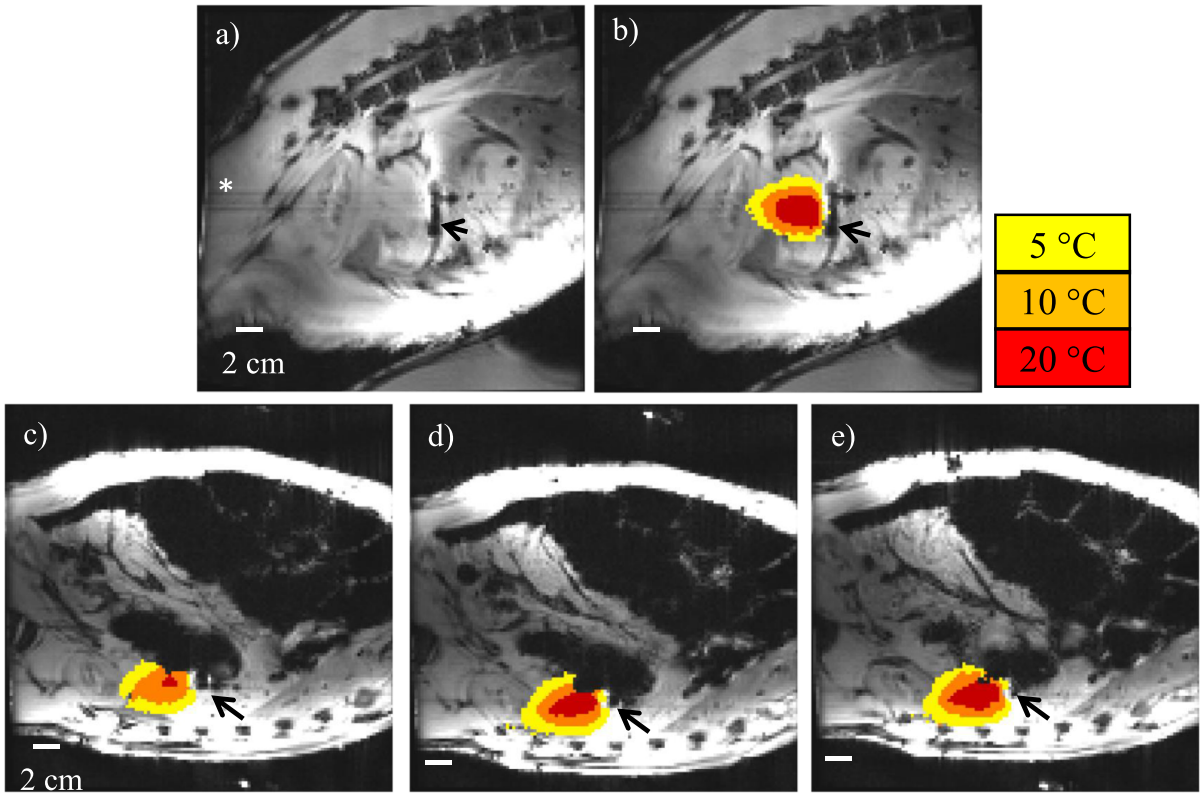

FIG. 7. (a) Following dual-planar applicator placement in the *ex vivo* stomach lumen for sonication of pancreatic tissue (Fig. 6), an oblique imaging slice was prescribed through the central axis of the applicator (black arrow) and used to prescribe three additional axial monitoring planes through the transducer stage, with slice placement shown by the saturation bands (asterisk). Temperature distributions for each monitoring slice [(b)–(e)] are shown at the end of the 13 min heat (4 W/cm^2 applied intensity), with a maximum temperature rise of ~40 °C.

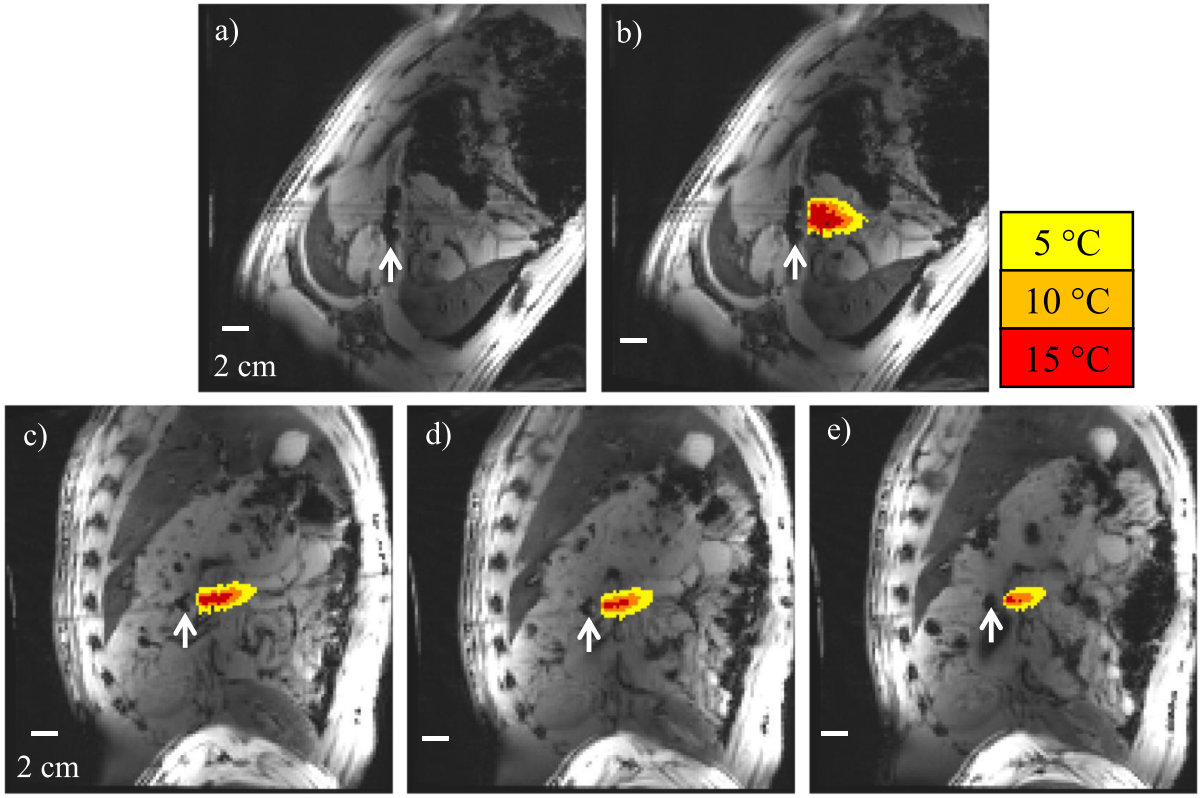

FIG. 8. (a) Placement of the dual-curvilinear endoluminal applicator (white arrow) in the *ex vivo* pig carcass stomach and sonication of adjacent pancreatic tissue. Real-time thermometry was monitored in a (b) sagittal slice through the applicator and [(c)–(e)] three axial slices orthogonal to the transducer stage. Sonication duration was 6 min at 4 W/cm^2 applied acoustic intensity and produced a maximum temperature elevation of 24 °C.

ablative ($\Delta T > 15$ °C) contour dimensions increased from 4 to 40 mm in length and 4–28 mm in width as the sonication time increased from 1 to 13 min, for applied surface intensities around 4 W/cm^2 (range: 3.8–5 W/cm^2). For the curvilinear applicator at 4 W/cm^2, $\Delta T > 15$ °C contours extended approximately 1–24 mm in length and 2–7 mm in width as the heating time increased from 1 to 6 min. Temperature standard deviation using the phased-array coil and surface coils varied between 0.2–0.3 and 2.2–4.0 °C, respectively.

3.C. MR-guided *in vivo* porcine experiments

Table II lists details for each *in vivo* animal experiment, including devices under test, sonication parameters, MRTI scheme, and MRTI/gross lesion measures. Oral, intraesophageal delivery of the dual-planar and curvilinear applicators under MR guidance into the stomach and positioning adjacent to the splenic lobe of the porcine pancreas were achieved in all experiments, as demonstrated in Fig. 9. Better success in mitigating susceptibility artifacts caused by bowel gas adjacent to the treatment site for clearer thermometry was achieved with the animal in dorsal recumbency as compared to left lateral recumbency.

Figure 10 illustrates MRTI temperature images from the second sonication in pancreatic tissue in Pig 1. A maximum temperature elevation of ~20 °C was generated in pancreatic tissue at a depth of about 17 mm from the transducer surface. This temperature maximum was reached and sustained after ~4 min of heating. Using the multiple-baselines

TABLE I. Experimental details and MRTI $T > 15$ °C contour dimensions for *ex vivo* porcine cadaver heating trials of pancreatic tissue.

Expt. No.	Device	Freq. (MHz)	Coil	Acoustic intensity (W/cm^2)	Time (min)	Max Temp. (°C)	Temp. Std. Dev. (°C)	Long. extent [5 min/t_{final}] (mm)	Transverse extent at 1 cm depth [5 min/t_{final}] (mm)	Transverse extent at 2 cm depth [5 min/t_{final}] (mm)
1	Curv.	3.3	Phased-array	4.0	6	22	0.3	[23/25]	[6/6]	[6/7]
2	Planar	3.2	Phased-array	4.0	13	40	0.2	[24/42]	[12/27]	[8/28]
3	Planar	3.2	Phased-array	3.8	5	25	0.3	23	11	10
4	Planar	3.2	Phased-array	4.5	10	40	0.2	[20/20]	[13/15]	[8/10]
5[a]	Planar	3.2	Surface/tracking	4.5	5	30	4.0	18	14	11
6	Planar	3.2	Surface/tracking	5	5	28	2.2	20	12	9

[a]Liver tissue targeted through the stomach was used as surrogate transgastric target similar to pancreas.

TABLE II. Sonication parameters and details for *in vivo* porcine pancreas heating experiments.

Pig	Device	Freq. (MHz)	Thermometry scheme	Son. site	Animal position	Acoustic intensity (W/cm^2)	Time (min)	Max Temp. (°C)	Temp. Std. Dev. (°C)	$T > 15$ °C dimensions (mm)[a]	Lesion dimensions (mm)[a]
1	Planar	3.2	Multislice/ multibaseline	1	Left lateral	5.5	10	NA	NA	NA	17 × 4 ×9
				2	Dorsal	5.5	16	20	3.0	15 × 7 × 8	16 × 4 × 10
2	Planar	3.2	Single-slice w/resp. gating	1	Dorsal	5.4	12	18	2.0	19 × NA × 7	22 × 10 × 6
				2	Dorsal	6.2	12	20	2.3	19 × NA × 9	28 × 8 × 5
3	Curv.	3.3	Single-slice w/resp. gating	1	Dorsal	6.2 6.9	9 6	17 16	0.8 0.8	12 × 3 × 6	NA

Note: NA = not available.
[a]Dimensions reported in length × width × depth.

reconstruction approach permitted recovery of temperature data for the entire treatment as shown in Fig. 10(e), by reducing motion-associated misregistration artifacts. There was general agreement in the temperature measurements recorded during breath-holds (where baseline misregistration would be minimal) and interim time-points. The temperature standard deviation was 3.0 °C using the multiple-baseline reconstruction, as compared to 4.5 °C using a single-baseline reconstruction.

Temperature profiles for heating trials using the dual-planar applicator in Pig 2 and the dual-curvilinear applicator in Pig 3 are illustrated in Fig. 11. MRTI in both experiments was performed using a single thermometry plane, with respiratory gating to minimize misregistration. This scheme permitted visualization of the entire course of heating during the treatment, with minimal motion-related artifacts. For the first treatment site in Pig 2, the maximum temperature elevation was ~18 °C at a depth of 20 mm from the transducer surface, and the temperature magnitude was responsive to increases in applied input power to the transducers, as shown in Fig. 11(b). For Pig 3, using the dual-curvilinear applicator, a maximum temperature elevation was ~17 °C was reached 16 mm from the transducer, and the temperature near the splenic vein immediately distal to the target region was reduced to ~5 °C. The temperature standard deviations for the thermometry in Pig 2 and 3 were 2.0–2.3 and 0.8 °C, respectively, as measured in the target region prior to the onset of heating. The greater temperature uncertainty in Pig 2 can likely be attributed to closer proximity of the target region to bowel tissue with large susceptibility artifacts. MRTI revealed moderate temperature penetration ($\Delta T_{max} > 10$ °C) beyond the pancreas boundaries for treatment site #2 for Pig 2, with preferential heating of spine tissue within 4 cm of and directly aligned with the applicator.

Following animal euthanasia and excision of the pancreas and adjacent stomach tissue, the presence of thermal lesions in the splenic lobe of the pancreas was confirmed for each animal. Figure 12 depicts an image of a representative thermal lesion from Pig 1, along with the corresponding section with H&E staining to visualize a contiguous volumetric zone of coagulative necrosis, which appeared paler in comparison to undamaged or normal tissue. Dimensions of the thermal lesions for each pig and sonication site, based on gross inspection, are given in Table II. For Pig 3, thermal lesion dimensions were not available from gross measurements and instead were estimated by $\Delta T > 15$ °C contours from MRTI. The length, width, and depth of the lesions from the surface of the pancreas ranged from 12 to 28 mm, 3 to 10 mm, and 5 to 10 mm, respectively. The width of the transition zone, forming the boundary between complete coagulation and normal tissue, was less than 2 mm for all cases. Inspection of excised stomach tissue revealed that samples from Pigs 1 and 3 possessed a slight discoloration on the exterior surface adjacent to the treated pancreas, and histological analysis confirmed areas of acute, sublethal thermal damage to portions of the outer muscular and serosal

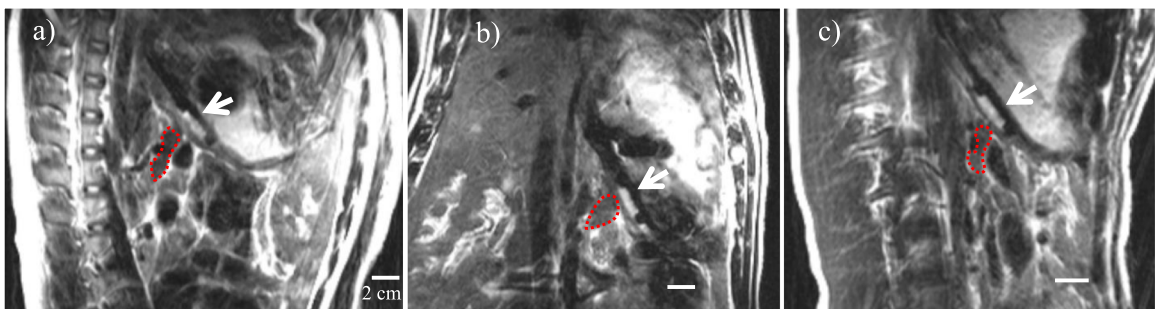

FIG. 9. T2-weighted sagittal MRI images illustrating placement and visualization of the planar [(a) and (b)] and curvilinear (c) endoluminal applicators (white arrow) in the stomach lumen adjacent to the splenic lobe of the pancreas (red dotted outline) in the three *in vivo* porcine experiments. (See color online version.)

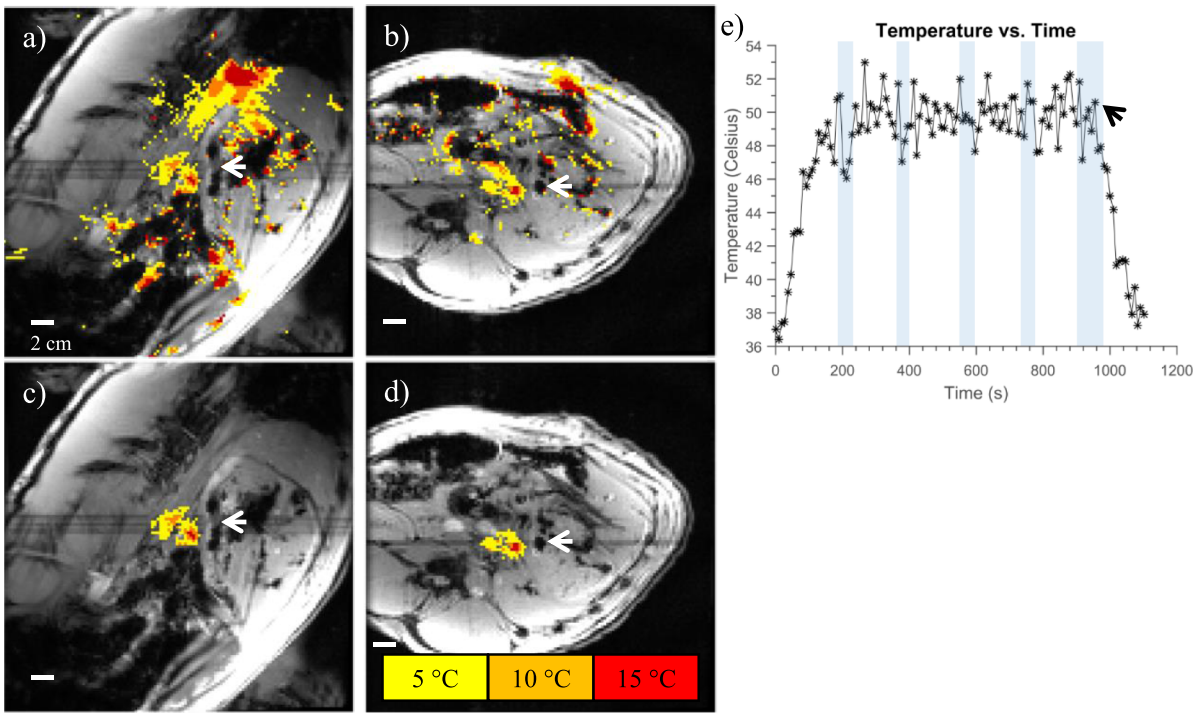

FIG. 10. (a) Sagittal and (b) axial temperature monitoring planes generated using a multiple-baseline reconstruction, for endoluminal sonication of pancreatic tissue *in vivo* in Pig 1 after 6 min of heating, at ~5.5 W/cm^2 applied to each transducer of the dual-planar applicator (white arrow). [(c) and (d)] For clarity, rectangular spatial-masks were applied to each image to isolate sonication-induced temperature change. (e) The temperature profile over time in a small (3×3 pixels) ROI in the heated region using the multiple-baseline reconstruction, illustrating prolonged temperature elevation of target tissue to around 50 °C, with the end of sonication indicated by the black arrow. Temperature measurements taken during breath-holds are contained within the shaded boxes.

layers. There was no observed lesion formation in tissues other than the stomach and pancreas during gross inspection at necropsy.

4. DISCUSSION

This study has demonstrated the basic feasibility of generating ablative temperature elevations and thermal lesions in the porcine pancreas through the stomach wall using an endoluminal ultrasound applicator under MR guidance. These POC MR-compatible applicators could be positioned under real-time MR guidance, through the GI tract and immediately adjacent to the pancreas target region. The feasibility of using MRTI techniques to permit multislice and real-time monitoring of temperature evolution during treatments was demonstrated. The planar and lightly curvilinear transducer designs were able to achieve ablative temperature elevation (>15 °C) in pancreatic tissue at depths of 2–4 cm from the luminal wall in *ex vivo* porcine carcass models. As shown by MRTI (Figs. 5 and 6; Table I) and the acoustic beam profiles (Fig. 3), the curvilinear transducers resulted in more spatially selective heating profiles that were narrower and more constant-width along the heating length relative to the planar applicator, as expected.[28] In the *in vivo* experiments, the maximum temperatures and extents of effective temperature elevations extended ~20 °C at depths up to 2 cm from the transducer surface, but were reduced compared to *ex vivo* studies. One likely cause for these discrepancies is the heat sink effect caused by general perfusion and the proximity of nearby major vasculature, i.e., the splenic vein and artery, which run along the length of the splenic lobe and were evident at a depth of 1.5–2 cm in the pancreas (Fig. 7). In the face of perfusion effects, greater applied powers or more focused transducer configurations could be utilized to increase heat generation. Coupling and positional alignment between the applicator, stomach lumen, and pancreatic tissue may also be inconsistent in the presence of respiratory motion, resulting in the dispersion of acoustic energy over a larger volume of tissue. Applicator fixation methods could alleviate this coupling issue, with potential strategies including distensible back balloons, clip fixation, or vacuum suction of the applicator against the stomach lumen. Incorporation of flexibility, steering, and placement strategies common to endoscopes into the flexible distal end of the device may also improve positioning and reduce movement. Further, variation in the lesion dimensions and shapes in the *ex vivo* and *in vivo* experiments may be attributed to the distinct anatomical conditions in each animal, as access to pancreatic tissue and the overall size of targetable tissue varied between animals (Fig. 7).

A primary safety concern affiliated with this endoluminal delivery of the thermal ablation approach is the preservation of the luminal wall from thermal injury, which could cause formation of a gastric fistula.[3] While MRTI in the *ex vivo* and *in vivo* studies illustrated that the water cooling was effectively pushing the maximum temperatures deeper into the tissue, there was some histological evidence of

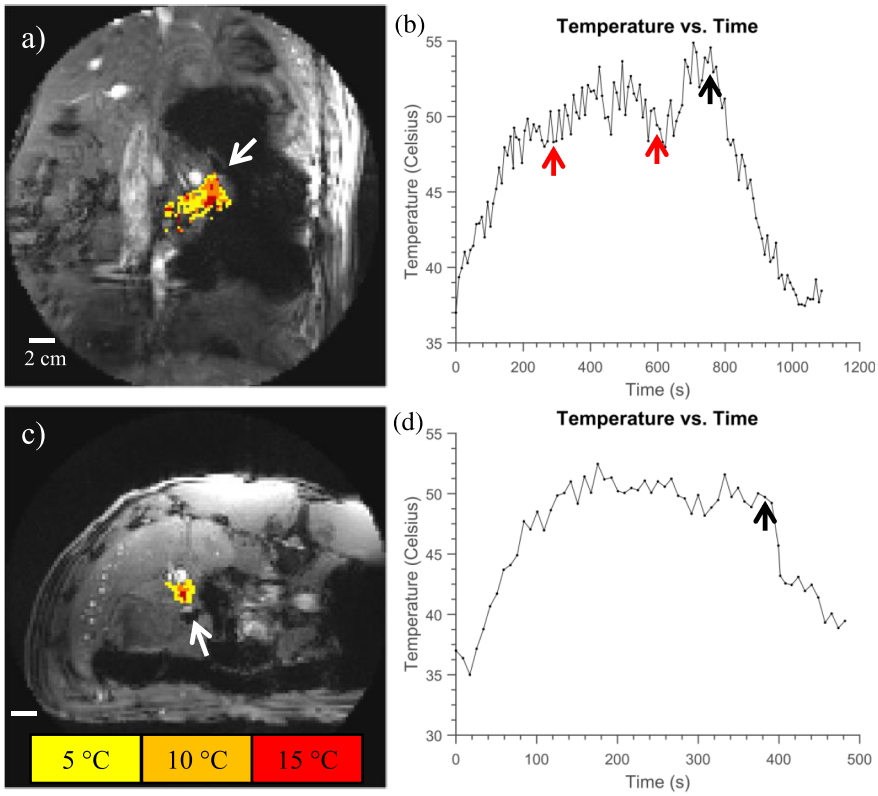

FIG. 11. End-sonication temperature distributions are shown for endoluminal heating of pancreatic tissue though the stomach lumen for (a) a sagittal monitoring slice of the dual-planar applicator in sonication site #1 for Pig 2 and (c) an axial monitoring slice of the dual-curvilinear applicator in Pig 3. For both experiments, MRTI was performed with a single monitoring slice and respiratory-gated acquisition. Temperature–time curves for small (3×3 pixels) ROIs in the heated region are shown in (b) and (d) for the dual-planar and dual-curvilinear heats, respectively. The transducers were driven at an average of 5.4 W/cm^2 for (a) and (b) and 6.9 W/cm^2 for (c) and (d). Time-points at which the applied power to the transducers was increased from 4.8 to 5.5 W/cm^2 and then from 5.5 to 6 W/cm^2 for Pig 2 are shown by the red arrows in (b), and the points at which power was switched off are indicated by the black arrows for both experiments. (See color online version.)

acute thermal damage to the outer muscular and serosal layers of excised stomach tissues from the *in vivo* studies. One likely cause for this is the large measured thickness (~8 mm) of the porcine stomach wall near the esophagus, where the sonications for treating the splenic lobe of the pancreas were performed. In theoretical simulations of endoluminal ultrasound ablation of human pancreatic cancer, while pertaining to different anatomical conditions and tissue properties compared to porcine anatomy, it was demonstrated that endoluminal sonication through thinner luminal walls results in lower temperatures within the wall and minimizes the risk of thermal injuries.[31] As such, the risk of thermal damage would be reduced in humans due to the lower anticipated luminal wall thicknesses (2–3 mm). Similarly, in the experimental porcine setting there was likely an increased effective acoustic attenuation and absorption in the wall tissue due to the presence of food particles and/or gas bubbles in the mucosal layers, which could be reduced by flushing the interior stomach or GI lumen via lavage prior to treatment.[17] Transducer design changes that would enable better sparing of thick luminal walls include incorporating more tightly focused designs, with the focus depth at least 1 cm beyond the wall tissue.[31] Improving coupling between the applicator cooling balloon and luminal wall through tip steering, compression, or fixation mechanisms may also provide for consistent or enhanced luminal sparing.

While the porcine represents a close animal model to humans in terms of digestive anatomy, key differences exist which present unique challenges as compared to the application of this technique in humans. In humans, the head of the pancreas is the largest region of the organ and the most common site for tumor genesis as compared to tail/body regions.[32] Treatment of tumors in the pancreatic head would ideally be performed with the endoluminal applicator positioned in the duodenal lumen (see Fig. 1), which is intimately attached to the head and would facilitate luminal sparing due to the thinner thickness of the duodenal wall (2 mm distended) as compared to the stomach wall (3–5 mm) in humans.[33–35] In the porcine model, the head of the pancreas (the duodenal lobe) is the smallest volumetric portion of the pancreas[36] and is separated from the medial duodenum by mesentery, leaving potential gaps between the two organs.[37] Further, the pyloric region that connects the stomach and duodenum contains a mucosal protuberance called the torus pyloricus, which results in much more constriction in the porcine model than in humans, impeding endoluminal access. As such, the splenic lobe of the porcine pancreas (analogous to the tail of the human pancreas) was chosen as the target region, due to its larger comparative volume and relative ease of access

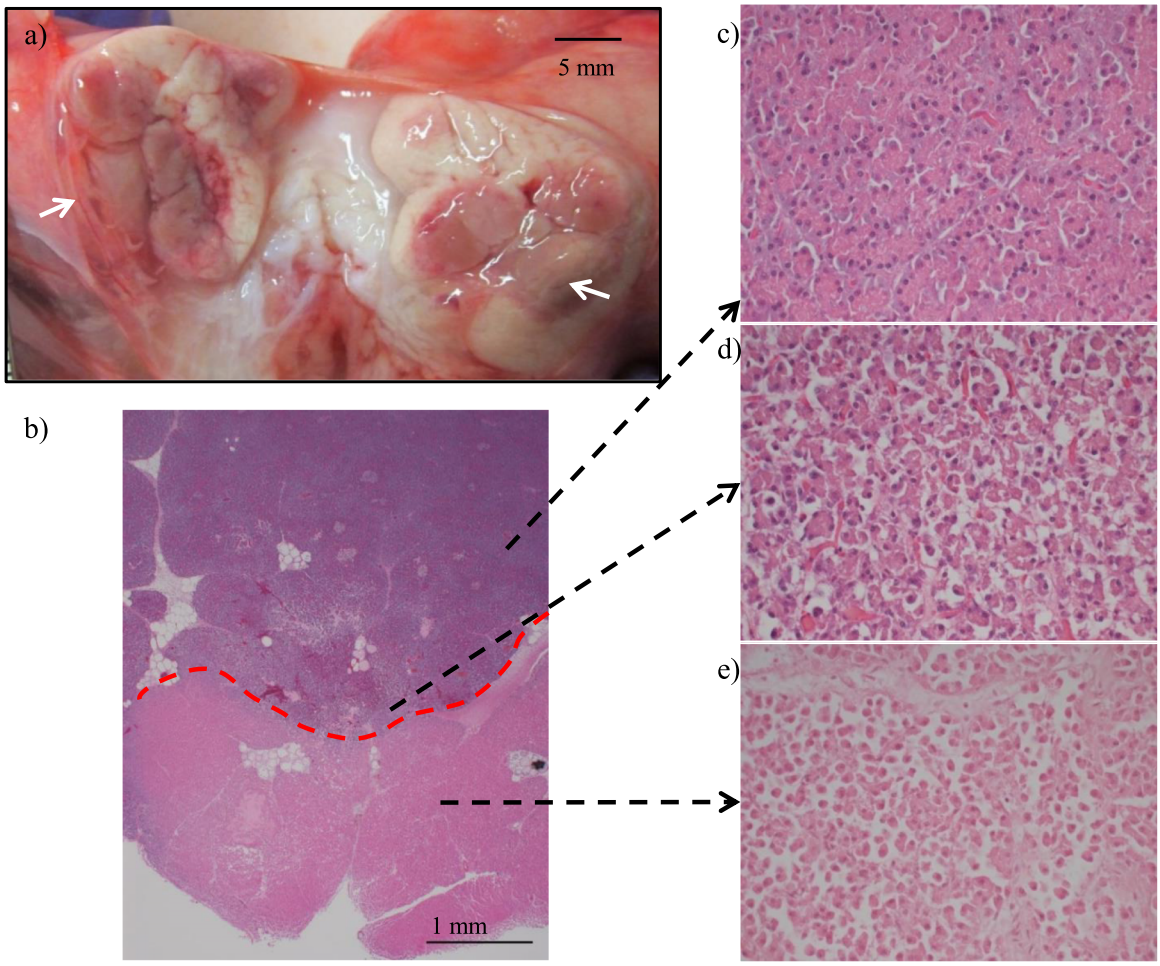

FIG. 12. Longitudinal section through a thermal lesion on the splenic lobe of the excised pancreas from an *in vivo* porcine study, revealing ablative penetration to a depth of ~1 cm from the pancreas surface, with direction of applied ultrasound shown by the white arrows. Pancreatic histopathology (b) illustrates the subgross or macroscopic histology of the pancreas and clearly depicts the boundaries of the thermal lesion (delineated by the red dashed line). Histological analysis of the pancreas was characterized by (c) untreated, normal pancreatic acini, (d) sublethally damaged lesion borders or transition zone, and (e) thermally ablated tissue that resulted in diffuse coagulation necrosis. [(b) = 2.5×, (c)–(e) = 40×. All slides were stained with H&E.] (See color online version.)

from the stomach lumen. Tradeoffs associated with this target choice include the greater susceptibility to respiratory motion in the tail region,[38] the thicker luminal walls adjacent to the tail relative to the stomach antrum or duodenum, and proximity to major vasculature and the left kidney, which act as heat sinks.

The endoluminal ultrasound applicators were designed for compatibility with MR guidance, which permitted target identification, device localization, and positioning, as well as direct treatment monitoring through PRF-based MRTI. Inclusion of the active tracking coils provided quick localization of the applicator and automated prescription of thermometry planes through the transducers, thereby reducing overall procedural times for a single device placement and sonication by approximately 5–10 min, as compared to manual methods. Hardware limitations of the MRI system in our current setup required that they could only be implemented with up to three individual surface coils for deep abdominal imaging, which suffered from poorer imaging quality and lower thermometry fidelity as compared to what could be achieved with the phased-array coil (Table I) and hence were unsuitable for the *in vivo* studies. With additional hardware to integrate the tracking coils with phased-array coil imaging, they could be valuable in reducing procedural times as well as further developed to track applicator motion *in vivo*, as a means of evaluating different fixation strategies or for gating sonications in the presence of significant motion.

Due to the relatively long durations (5–15 min) of active sonications associated with this volumetric heating strategy, multislice MRTI is a valuable and appropriate tool for monitoring the complete extent of heating over time. MRTI performed in the *ex vivo* studies using the phased-array coil permitted real-time and clear demarcation of temperature contour evolution, with the only significant noise source being susceptibility artifacts caused by gas in nearby bowel tissue. As anticipated, MRTI in the *in vivo* study suffered from additional respiratory motion artifacts, as well as flow artifacts from nearby major vasculature. While there was general agreement between the gross lesion measurements and MRTI ($\Delta T > 15\,^{\circ}\mathrm{C}$) measurements (Table II), discrepancies were expected due to limited thermometry precision as well as the inherent difficulty in registering the temperature monitoring

planes and lesion cutting planes, particularly as the orientation, shape, and position of the inspected tissues shift during excision. Both multiple-baseline reconstruction (Fig. 10) and respiratory gating (Fig. 11), using controlled respiration and pressure bellow input signal, were demonstrated to reduce motion artifacts for clearer real-time monitoring of thermometry during treatments. Compared to multiple-baseline reconstruction, the respiratory-gated acquisition scheme permitted more precise thermometry (Table II) and could be similarly adapted for multiple-plane monitoring at the cost of temporal resolution.[39,40] The multiple-baseline reconstruction methods as applied also have errors in temperature measurements immediately adjacent to the applicator, due to either different circulatory flow conditions or the development of temperature gradients caused by cooling water circulation throughout the duration of baseline collection. Besides motion compensation, other sources of significant artifacts, such as excessive gas in the stomach/bowels and peristalsis motion, could be reduced in future studies by flushing and filling the stomach with degassed water prior to treatment[17] and by administration of anticholinergic drugs, such as dicyclomine,[41] respectively. Although not demonstrated in this study, a substantial benefit of MRTI-based thermometry that could be applied in future studies is the real-time calculation of thermal dose accumulation in tissues, and inclusion of feedback control schemes based on temperature/dose levels in target or sensitive tissues to modulate applied power levels and/or applicator positioning.[30,42–45]

The primary outcome of this preliminary investigation was demonstration of the basic feasibility of placement, targeting and generating ablation in the pancreas under endoluminal device placement and MR/MRTI guidance. Substantial experimental variations and challenges were encountered in each animal study as we demonstrated feasibility, making clear definition of relationships between sonication parameters (durations, powers, and transducer geometries) and resulting lesion formation difficult at this time. Future validation studies can be applied to more clearly assess the safety and efficacy of this endoluminal approach using additional acute and chronic *in vivo* porcine studies. Further development and refinement of applicator designs and experimental methods should permit more reproducible experimental conditions and characterization studies to elucidate clearer relationships between sonication parameters, resulting temperature/thermal dose distributions, and lesion dimensions. These studies should permit formation of a consistent set of treatment parameters and methods, which can be evaluated in comprehensive safety studies to assess any acute and long-term complications resulting from the endoluminal ablation, as well as to evaluate thermal damage to the stomach and other tissues adjacent to the pancreas. Furthermore, as an alternative to ablation, further development of this approach could also be directed towards delivering moderate (40–45 °C) hyperthermia in the pancreas, which would benefit from the volumetric nature of heating and MR temperature monitoring and could potentially enhance drug delivery, chemotherapy, or radiation therapies in patients with PDAC.

5. CONCLUSIONS

The results of this study demonstrate preliminary feasibility that MR-guided endoluminal ultrasound applicators can generate volumetric thermal therapy in pancreatic tissues from within the GI tract. MR guidance provides an effective means of localizing and positioning the applicator in the GI tract for targeting pancreatic tissues and has the potential to enable conformal therapies through monitoring volumetric temperature elevation. Further development of this approach, including treatment control, validation, and refinement to applicator design and MR thermometry techniques, is warranted for preclinical evaluation.

ACKNOWLEDGMENTS

The authors would like to acknowledge Yamil Saenz for oversight of the surgical prep and anesthesia in the animal studies. The work was supported by National Institutes of Health Grant No. P01CA159992. This research was conducted with government support under and awarded by DOD, Air Force Office of Scientific Research, National Defense Science and Engineering Graduate (NDSEG) Fellowship, 32 CFR 168a. The authors alone are responsible for the content and writing of the paper.

CONFLICT OF INTEREST DISCLOSURE

The authors have no COI to report.

[a]Author to whom correspondence should be addressed. Electronic mail: matt.adams@ucsf.edu; Telephone: (415) 476-8639.

[1]S. Rombouts, J. Vogel, H. van Santvoort, K. van Lienden, R. van Hillegersberg, O. Busch, M. Besselink, and I. Molenaar, "Systematic review of innovative ablative therapies for the treatment of locally advanced pancreatic cancer," Br. J. Surg. **102**, 182–193 (2015).

[2]J. Vidal-Jove, E. Perich, and M. A. del Castillo, "Ultrasound guided high intensity focused ultrasound for malignant tumors: The Spanish experience of survival advantage in stage III and IV pancreatic cancer," Ultrason. Sonochem. **27**, 703–706 (2015).

[3]Y. Zhou, "High-intensity focused ultrasound treatment for advanced pancreatic cancer," Gastroenterol. Res. Pract. **2014**, 1–11.

[4]L. L. Xiong, J. H. Hwang, X. B. Huang, S. S. Yao, C. J. He, X. H. Ge, H. Y. Ge, and X. F. Wang, "Early clinical experience using high intensity focused ultrasound for palliation of inoperable pancreatic cancer," J. Pancreas **10**, 123–129 (2009).

[5]M. G. Keane, K. Bramis, S. P. Pereira, and G. K. Fusai, "Systematic review of novel ablative methods in locally advanced pancreatic cancer," World J. Gastroenterol. **20**, 2267–2278 (2014).

[6]R. Pezzilli, C. Ricci, C. Serra, R. Casadei, F. Monari, M. D'Ambra, R. Corinaldesi, and F. Minni, "The problems of radiofrequency ablation as an approach for advanced unresectable ductal pancreatic carcinoma," Cancers **2**, 1419–1431 (2010).

[7]R. Girelli, I. Frigerio, R. Salvia, E. Barbi, P. Tinazzi Martini, and C. Bassi, "Feasibility and safety of radiofrequency ablation for locally advanced pancreatic cancer," Br. J. Surg. **97**, 220–225 (2010).

[8]E. S. Ebbini and G. Ter Haar, "Ultrasound-guided therapeutic focused ultrasound: Current status and future directions," Int. J. Hyperthermia **31**, 77–89 (2015).

[9]Y. Kim, "Advances in MR image-guided high-intensity focused ultrasound therapy," Int. J. Hyperthermia **31**, 225–232 (2015).

[10]M. Anzidei, B. C. Marincola, M. Bezzi, G. Brachetti, F. Nudo, E. Cortesi, P. Berloco, C. Catalano, and A. Napoli, "Magnetic resonance-guided high-intensity focused ultrasound treatment of locally advanced pancreatic

adenocarcinoma: Preliminary experience for pain palliation and local tumor control," Invest. Radiol. **49**, 759–765 (2014).
[11]F. Wu, Z. Wang, H. Zhu, W. Chen, J. Zou, J. Bai, K. Li, C. Jin, F. Xie, and H. Su, "Feasibility of US-guided high-intensity focused ultrasound treatment in patients with advanced pancreatic cancer: Initial experience," Radiology **236**, 1034–1040 (2005).
[12]V. A. Salgaonkar and C. J. Diederich, "Catheter-based ultrasound technology for image-guided thermal therapy: Current technology and applications," Int. J. Hyperthermia **31**, 203–215 (2015).
[13]C. Lafon, Y. Theillere, F. Prat, A. Arefiev, J. Chapelon, and D. Cathignol, "Development of an interstitial ultrasound applicator for endoscopic procedures: Animal experimentation," Ultrasound Med. Biol. **26**, 669–675 (2000).
[14]D. Melodelima, F. Prat, J. Fritsch, Y. Theillere, and D. Cathignol, "Treatment of esophageal tumors using high intensity intraluminal ultrasound: First clinical results," J. Transl. Med. **6**, 28 (2008).
[15]M. Pioche, C. Lafon, E. Constanciel, A. Vignot, A. Birer, R. Gincul, V. Lepilliez, F. Prat, S. Roman, J. Y. Chapelon, J. C. Saurin, and T. Ponchon, "High-intensity focused ultrasound liver destruction through the gastric wall under endoscopic ultrasound control: First experience in living pigs," Endoscopy **44**(Suppl. 2), E376–E377 (2012).
[16]D. Melodelima, R. Salomir, J. Chapelon, Y. Theillère, C. Moonen, and D. Cathignol, "Intraluminal high intensity ultrasound treatment in the esophagus under fast MR temperature mapping: *In vivo* studies," Magn. Reson. Med. **54**, 975–982 (2005).
[17]T. Li, T. Khokhlova, E. Maloney, Y. Wang, S. D'Andrea, F. Starr, N. Farr, K. Morrison, G. Keilman, and J. H. Hwang, "Endoscopic high-intensity focused US: Technical aspects and studies in an *in vivo* porcine model (with video)," Gastrointest. Endosc. **81**, 1243–1250 (2015).
[18]M. A. Lewis, R. M. Staruch, and R. Chopra, "Thermometry and ablation monitoring with ultrasound," Int. J. Hyperthermia **31**, 163–181 (2015).
[19]N. J. McDannold and F. A. Jolesz, "Magnetic resonance image-guided thermal ablations," Top. Magn. Res. Imaging **11**, 191–202 (2000).
[20]B. D. De Senneville, C. Mougenot, B. Quesson, I. Dragonu, N. Grenier, and C. T. Moonen, "MR thermometry for monitoring tumor ablation," Eur. Radiol. **17**, 2401–2410 (2007).
[21]J. G. Fortner, D. S. Klimstra, R. T. Senie, and B. J. Maclean, "Tumor size is the primary prognosticator for pancreatic cancer after regional pancreatectomy," Ann. Surg. **223**, 147–153 (1996).
[22]S. Eroglu, B. Gimi, B. Roman, G. Friedman, and R. L. Magin, "NMR spiral surface microcoils: Design, fabrication, and imaging," Concepts Magn. Reson., Part B **17**, 1–10 (2003).
[23]H. F. Stewart, "Ultrasonic measurement techniques and equipment output levels," in *Essentials of Medical Ultrasound* (Humana, Clifton, NJ, 1982), pp. 77–116.
[24]C. L. Dumoulin and R. D. Darrow, U.S. patent No. 6,289,233 (11 September 2001).
[25]C. L. Dumoulin, R. P. Mallozzi, R. D. Darrow, and E. J. Schmidt, "Phase-field dithering for active catheter tracking," Magn. Reson. Med. **63**, 1398–1403 (2010).
[26]S. Roujol, M. Ries, B. Quesson, C. Moonen, and B. Denis de Senneville, "Real-time MR-thermometry and dosimetry for interventional guidance on abdominal organs," Magn. Reson. Med. **63**, 1080–1087 (2010).
[27]S. Elayaperumal, J. C. Plata, A. B. Holbrook, Y. Park, K. B. Pauly, B. L. Daniel, and M. R. Cutkosky, "Autonomous real-time interventional scan plane control with a 3-D shape-sensing needle," IEEE Trans. Med. Imaging **33**, 2128–2139 (2014).
[28]A. B. Ross, C. J. Diederich, W. H. Nau, V. Rieke, R. K. Butts, G. Sommer, H. Gill, and D. M. Bouley, "Curvilinear transurethral ultrasound applicator for selective prostate thermal therapy," Med. Phys. **32**, 1555–1565 (2005).
[29]K. K. Vigen, B. L. Daniel, J. M. Pauly, and K. Butts, "Triggered, navigated, multi-baseline method for proton resonance frequency temperature mapping with respiratory motion," Magn. Reson. Med. **50**, 1003–1010 (2003).
[30]B. D. De Senneville, C. Mougenot, and C. T. Moonen, "Real-time adaptive methods for treatment of mobile organs by MRI-controlled high-intensity focused ultrasound," Magn. Reson. Med. **57**, 319–330 (2007).
[31]M. S. Adams, S. J. Scott, V. A. Salgaonkar, G. Sommer, and C. J. Diederich, "Thermal therapy of pancreatic tumors using endoluminal ultrasound: Parametric and patient-specific modeling," Int. J. Hyperthermia **32**, 97–111 (2016).
[32]A. Stathis and M. J. Moore, "Advanced pancreatic carcinoma: Current treatment and future challenges," Nat. Rev. Clin. Oncol. **7**, 163–172 (2010).
[33]G. Masselli, A. Picarelli, M. Di Tola, V. Libanori, G. Donato, E. Polettini, A. Piermattei, P. Palumbo, A. Pittalis, and A. Saponara, "Celiac disease: Evaluation with dynamic contrast-enhanced MR imaging," Radiology **256**, 783–790 (2010).
[34]K. Nylund, T. Hausken, S. Ødegaard, G. Eide, and O. Gilja, "Gastrointestinal wall thickness measured with transabdominal ultrasonography and its relationship to demographic factors in healthy subjects," Ultraschall Med. **33**, E225–E232 (2012).
[35]I. Zuber-Jerger, A. Muller, F. Kullmann, C. M. Gelbmann, E. Endlicher, U. Muller-Ladner, and M. Fleck, "Gastrointestinal manifestation of systemic sclerosis–thickening of the upper gastrointestinal wall detected by endoscopic ultrasound is a valid sign," Rheumatology **49**, 368–372 (2010).
[36]J. Ferrer, W. E. Scott 3rd, B. P. Weegman, T. M. Suszynski, D. E. Sutherland, B. J. Hering, and K. K. Papas, "Pig pancreas anatomy: Implications for pancreas procurement, preservation, and islet isolation," Transplantation **86**, 1503–1510 (2008).
[37]R. S. Date, J. Biggins, I. Paterson, J. Denton, R. F. McMahon, and A. K. Siriwardena, "Development and validation of an experimental model for the assessment of radiofrequency ablation of pancreatic parenchyma," Pancreas **30**, 266–271 (2005).
[38]D. K. Bhasin, S. S. Rana, and V. S. Chandail, "The pancreas and respiration: Oblivious to the obvious," J. Pancreas **7**, 578–583 (2006).
[39]C. Weidensteiner, B. Quesson, B. Caire-Gana, N. Kerioui, A. Rullier, H. Trillaud, and C. T. Moonen, "Real-time MR temperature mapping of rabbit liver *in vivo* during thermal ablation," Magn. Reson. Med. **50**, 322–330 (2003).
[40]S. Morikawa, T. Inubushi, Y. Kurumi, S. Naka, K. Sato, K. Demura, T. Tani, and H. A. Haque, "Feasibility of respiratory triggering for MR-guided microwave ablation of liver tumors under general anesthesia," Cardiovasc. Intervent. Radiol. **27**, 370–373 (2004).
[41]L. Marti-Bonmati, M. Graells, and C. Ronchera-Oms, "Reduction of peristaltic artifacts on magnetic resonance imaging of the abdomen: A comparative evaluation of three drugs," Abdom. Imaging **21**, 309–313 (1996).
[42]R. Salomir, F. C. Vimeux, J. A. de Zwart, N. Grenier, and C. T. Moonen, "Hyperthermia by MR-guided focused ultrasound: Accurate temperature control based on fast MRI and a physical model of local energy deposition and heat conduction," Magn. Reson. Med. **43**, 342–347 (2000).
[43]A. Vanne and K. Hynynen, "MRI feedback temperature control for focused ultrasound surgery," Phys. Med. Biol. **48**, 31–43 (2002).
[44]R. Chopra, M. Burtnyk, M. A. Haider, and M. J. Bronskill, "Method for MRI-guided conformal thermal therapy of prostate with planar transurethral ultrasound heating applicators," Phys. Med. Biol. **50**, 4957–4975 (2005).
[45]E. Delabrousse, R. Salomir, A. Birer, C. Paquet, F. Mithieux, J. Chapelon, F. Cotton, and C. Lafon, "Automatic temperature control for MR-guided interstitial ultrasound ablation in liver using a percutaneous applicator: *Ex vivo* and *in vivo* initial studies," Magn. Reson. Med. **63**, 667–679 (2010).